

Developing a Novel Image Marker to Predict the Responses of Neoadjuvant Chemotherapy (NACT) for Ovarian Cancer Patients

Ke Zhang^{a,b*}, Neman Abdoli^{b*}, Patrik Gilley^b, Youkabed Sadri^b, Xuxin Chen^b, Theresa C. Thai^c, Lauren Dockery^d, Kathleen Moore^d, Robert S. Mannel^d, Yuchen Qiu^{a,b,1}

^a Stephenson School of Biomedical Engineering, University of Oklahoma, Norman, OK, USA
73019

^b School of Electrical and Computer Engineering, University of Oklahoma, Norman, OK,
USA 73019

^c Department of Radiology, University of Oklahoma Health Sciences Center, Oklahoma City,
OK, USA 73104

^d Department of Obstetrics and Gynecology, University of Oklahoma Health Sciences Center,
Oklahoma City, OK, USA 73104

ABSTRACT

Objective: Neoadjuvant chemotherapy (NACT) is one kind of treatment for advanced stage ovarian cancer patients. However, due to the nature of tumor heterogeneity, the patients' responses to NACT varies significantly among different subgroups. To address this clinical challenge, the purpose of this study is to develop a novel image marker to achieve high accuracy response prediction of the NACT at an early stage.

Methods: For this purpose, we first computed a total of 1373 radiomics features to quantify the tumor characteristics, which can be grouped into three categories: geometric, intensity, and texture features. Second, all these features were optimized by principal component analysis algorithm to generate a compact and informative feature cluster. Using this cluster as the input, an SVM based classifier was developed and optimized to create a final marker, indicating the likelihood of the patient being responsive to the NACT treatment. To validate this scheme, a total of 42 ovarian cancer patients were retrospectively collected. A nested leave-one-out cross-validation was adopted for model performance assessment.

Results: The results demonstrate that the new method yielded an AUC (area under the ROC [receiver characteristic operation] curve) of 0.745. Meanwhile, the model achieved overall accuracy of 76.2%, positive predictive value of 70%, and negative predictive value of 78.1%.

Conclusion: This study provides meaningful information for the development of radiomics based image markers in NACT response prediction.

Keywords: Radiomics, ovarian cancer, computer aided detection, neoadjuvant chemotherapy

¹ Corresponding author: qiuyuchen@ou.edu *Both Ke Zhang and Neman Abdoli are considered first authors.

1. INTRODUCTION

Being the most lethal gynecological malignancy, it is anticipated that 19710 patients will be newly diagnosed with ovarian cancer in 2023 within United States, while 13270 patients may be died from ovarian carcinoma this year [1]. Since most patients are diagnosed at an advanced stage (III or IV) [2, 3], the current standard primary treatment is primary debulking surgery (PDS) [4] to remove as many tumors as possible, followed by a postoperative adjuvant chemotherapy to target the residual cancer cells and reduce the recurrence risk. However, PDS is not suitable when unresectable tumor is diagnosed, or patient can't tolerate aggressive surgeries[5]. As an effective and milder alternative to PDS, neoadjuvant chemotherapy (NACT) [6-8] first administrates several cycles of chemotherapy, after which the interval debulking surgery (IDS) is performed. As compared to PDS, the benefits of NACT have been demonstrated by many investigations [6, 9-13], including less tissue resection and shorter operation time.

However, not all patients will be responsive to the NACT therapy [14]. Although NACT is performed, tumors may continue progressing, while some severe side effects may still occur on the patients [15]. As a result, some possible PDS candidates may be completely ineligible after NACT therapy. Additionally, the resistance to chemotherapy possibly driven by NACT is still a contentious but noticeable issue [16]. Therefore, to achieve an optimal treatment outcome, it is of crucial importance to investigate NACT prognostic models. Accordingly, different approaches have been explored to predict the outcome of NACT treatments, which are based on the FIGO (International Federation of Gynecology and Obstetrics) staging [17], demographic information [18], radiology findings[19, 20], CA-125 (cancer antigen 125) [21, 22], HE4 (Human Epididymis Protein 4) [23], BRCA 1/2 gene mutations [24], and so forth. However, due to the limited reliability and robustness of these models, they are not yet widely recognized [19, 25] in clinical practice.

Meanwhile, among all these technologies used in the prognostic assessment, computed tomography (CT) scan [26] has its unique superiority over the others due to its advantages of wide availability and low operating cost [27, 28]. Moreover, radiomics[29-31], a recent emerging approach, can extract and quantify the tumor characteristics from CT images, aiming to uncover the underlying biology mechanism which is associated with patient's diagnosis or prognosis. Although this method has been applied in various scenarios, few research have been conducted on using this novel technique for NACT prediction in ovarian cancer treatment. In this investigation, we aim to develop a radiomics based CT image marker to achieve high accuracy prediction of NACT responses. All the details are presented in the following sections.

2. MATERIALS AND METHODS

2.1 Database

This retrospective dataset contains a total of 42 advanced stage ovarian cancer patients, among which 14 patients are responders who achieved optimal debulking after NACT treatment and the rest of the patients are non-responders. All the selected patients were diagnosed with recurrent epithelial ovarian cancer (EOC), and had received NACT therapy before IDS, which were performed at the University of Oklahoma Health Sciences Center. The patients' histology types include endometrial, serous, clear cell, and mucinous. For each patient, we collected the pre-therapy CT images following the standard acquisition protocols. Specifically, the image obtainment was conducted on a GE LightSpeed VCT 64-detector or GE Discovery 600 16-detector CT machines. X-ray tube current was set to be from 100 to 600 mA to fit the various body size, with a tube power of 120 kVp. The examination was conducted by the following procedures: The contrast agent (Isovue 370, 100 cc) was first injected to the patient intravenously at a rate of 2–3 cc per second. The initial scan started 60 seconds after injection began, while the second scan started 5 minutes after the completion of injection. CT images were reconstructed to 1.25 mm in axial axis, and 2.5 mm in sagittal and coronal directions.

2.2 Image Feature Computation

Prior to the image feature computation, we performed tumor segmentation on each case to generate the 3D volume of interest (VOI). An experienced radiologist identified each tumor on the acquired CT images and attached annotation to the image showing the largest tumor area. With the reference of the annotation, all the slices containing metastatic tumors can be determined accurately and processed by a previously developed segmentation algorithm[32], which combines a multilayer topographic region growth algorithm with adaptive thresholds and a dynamic edge tracking method. Due to the heterogeneity of metastatic tumors, the automated segmentation results may not be adequately accurate for the following process. Therefore, the automatic segmentation results were visually evaluated by experienced researchers and the tumor contours may be manually corrected if needed.

Next, a large amount of radiomics features were computed from the segmented tumors based on the original CT images, using an open-source platform Pyradiomics[33]. Three categories of features were computed, namely, shape, first order features, and texture features. The shape features characterize the 3D size and geometry of the lesion from diverse perspectives, such as voxel volume and elongation. First order features depict the intensity distribution of the voxels inside the segmented VOI. The texture features include gray level co-occurrence matrix (GLCM) features[34], gray level dependence matrix (GLDM) features[35], gray level run length matrix (GLRLM) features[36], gray level size zone matrix (GLSZM) features[37], and neighboring gray tone difference matrix (NGTDM) features[38]. These features enable a quantitative depiction of the tumor textures by assessing the spatial distribution and variation of voxel values. For instance, GLDM features are generated from a matrix that describes the appearance of qualified neighboring voxels surrounding the central voxel to measure the dependency relationships across intensity levels. Furthermore, we also obtained extra first order and texture features from several filtered image types: exponential, gradient, local binary pattern 3D (LBP3D), logarithm, square, square root, and wavelet filters. In summary, a total of 1373

features extracted from the smallest tumor in each case were utilized for training the model, as illustrated in table 1.

Table 1. The number of features of different image types and feature types used in this study.

Image Type	Feature Type							Total
	Shape	First order	GLCM	GLDM	GLRLM	GLSZM	NGTDM	
Original	14	18	24	14	16	16	5	107
Exponential	0	16	0	7	8	3	0	34
Gradient	0	18	24	14	16	16	5	93
LBP3D	0	45	21	14	16	16	5	117
Logarithm	0	18	24	14	16	16	5	93
Square	0	17	24	14	16	16	5	92
Square root	0	18	24	14	16	16	5	93
Wavelet	0	144	192	112	128	128	40	744
Total	14	294	333	203	232	227	70	1373

2.3 Develop a Machine Learning based Model to Predict the Response of NACT

Using the established feature pool, we developed a classification model with scikit-learn [39] to predict the NACT response for each individual patient (Figure 1). At the onset of the model, all the features were first scaled by the following formula: $\mathbf{x}' = (\mathbf{x} - \mu)/\sigma$, where \mathbf{x} is a vector containing original values of a feature, μ and σ are the corresponding mean and standard deviation calculated from training set, respectively. Given the imbalanced nature of the dataset, the SMOTE (synthetic minority over-sampling technique) was employed to augment data in the minority class [40]. In this method, it first selects a sample \mathbf{x}'_r from the randomly shuffled minority class. Using \mathbf{x}'_r as a reference point, the algorithm locates its k nearest neighbors in minority group. A new sample \mathbf{x}'_s will then be synthesized by the following formula: $\mathbf{x}'_s = \mathbf{x}'_r + \beta(\mathbf{x}'_i - \mathbf{x}'_r)$, where \mathbf{x}'_i is one of the k nearest neighbors and β is randomly determined within the range (0, 1). This synthetic process will persist until the minority dataset is augmented to the balanced level.

Next, feature dimension reduction was conducted using principal component analysis (PCA) [41] on the training matrix \mathbf{X}' . PCA generates the principal components (PCs) based on the co-variance matrix $\mathbf{M} = \mathbf{X}'^T \mathbf{X}'$. Each PC is an eigenvector of the matrix \mathbf{M} representing a direction in the redefined feature space, while the variance explained by this PC is represented by its corresponding eigenvalue. Based on the spectral theorem [42], these variances quantifies the importance of each PC to the matrix, which were organized in descending order. Since the variance decreases significantly, it becomes feasible to use only a small portion of the most important PCs to approximate the original feature vectors with a satisfactory accuracy [41]. Accordingly, we restricted the original data dimension under 10 by PCA prior to classification.

After that, a linear support vector machine (SVM) classifier [43] was implemented to distinguish the responders and non-responders from the dataset. As a widely used supervised classification algorithm, SVM has demonstrated its effectiveness when working with small size datasets [44]. In binary classification tasks, rather than just finding one hyperplane that simply separates the two classes, SVM seeks an optimal hyperplane that has the largest margin between

the two classes, relying on the samples closest to the hyperplane (i.e., support vectors). Meanwhile, a regularization item is incorporated into the objective function as a soft margin constraint to mitigate overfitting on outliers that are located very close to the opposing class. The feature process pipeline of this machine learning model is depicted in Fig. 1a.

Finally, we employed a nested leave-one-out cross-validation (LOOCV) [45, 46] to evaluate the classification performance of this SVM-based model (Figure 1b). LOOCV is a unique type of cross-validation technique, in which the testing set only contains one case and all the remaining cases are used to train the model. This approach can maximally eliminate the random partition of the dataset and produces an almost unbiased evaluation result [47]. However, since hyperparameter tuning was also implemented within the LOOCV process, it incorporates testing data into model training, which may result in overestimating the model’s generalization performance. Thus, we introduced the nested LOOCV with 2 levels: the outer LOOCV is solely responsible for the evaluation while the inner LOOCV is embedded within the outer LOOCV to fine-tune the hyperparameters of related modules, including SMOTE, PCA, and SVM. This nested structure effectively decouples the testing data from training data, leading to a significant decrease in evaluation bias, and bringing error estimation close to the true level. The model performance was assessed by the receiver operating characteristic (ROC) curve[48], and metrics such as the area under curve (AUC) [49] value and overall accuracy (ACC) were estimated.

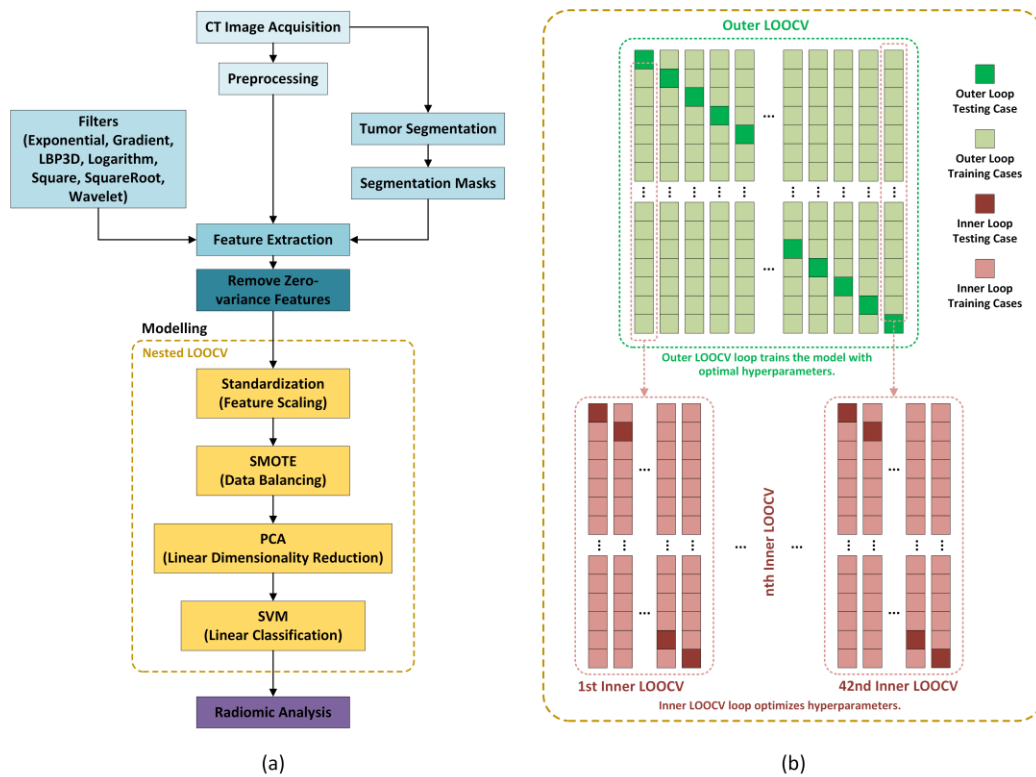


Fig. 1. Pipeline of the radiomic analysis in this study.

3. RESULTS

Figure 2 demonstrates one sample case of tumor segmentation results as well as 6 of the extracted 1373 features from this tumor. All the CT images containing this tumor are displayed from left to right in the first row, and the outline of the ROI tightly wrapping the tumor tissue in each image is identified and marked by red color. The tumor in each CT image is isolated and illustrated in the second row which contains all the information that is going to be extracted for this case. The 3D shape of the tumor is shown in the third row with 6 extracted logarithm and gradient features as examples.

The hierarchically clustered heatmap [50] of Pearson's correlation coefficients for the extracted 1373 radiomic features is demonstrated in Figure 3, with the values ranging from -1 to 1. The negative value is represented using a brown color, while the positive value is represented by a green color. The deeper color indicates a larger absolute value of the correlation coefficient. The entire heatmap shows that the feature correlations are relatively low, and the dendrogram indicates that the associations occur on the features from different categories. Figure 4 provides the distributions of correlation values between features of the same feature type or image type. From Figure 4a, we can observe that the features within most subgroups have low association, while the only exception is the shape features. When sorting the features based on image types (Figure 4b), it becomes evident that certain features extracted from the same filtered image exhibit relatively higher correlations with each other, and the others are still remaining low. For example, the median correlation coefficient of the features calculated from gradient filter processed images is approximately 0.38, while this value is only 0.23 for the wavelet filter subgroup. Figure 5 plots the histogram of the absolute values of all the calculated correlation coefficients. We can observe that 90.2 % of the correlation coefficient values are less than or equal to 0.5. The results indicate that the extracted 1373 raw features contain comprehensive information describing tumor attributes with negligible redundancy at the same time.

Table 2 summarizes and compares the model performance when only using one type of the features. The GLSZM feature performs best among all different categories, yielding an AUC value of 0.638 ± 0.094 and an ACC value of 71.4 %. Meanwhile, the GLCM features achieves the second-highest performance, with AUC and accuracy values of 0.633 and 64.3 %, respectively. Similarly, the shape and first order features can still distinguish the positive cases from negative cases to a certain extent, resulting in AUC values of 0.617 and 0.559 respectively. In contrast, the other feature classes did not show significant discriminative powers. Figure 6 demonstrates the averaged weight of different feature types applying on the PCA-generated new features, when using all the 1373 features in the final cluster. It reflects that the features from different subcategories have approximately equal contributions, with the GLDM and GLRLM contributing slightly more than the others.

The ROC curve and confusion matrix used to evaluate the performance of the model trained with 1373 features are plot in Figure 7. The corresponding AUC value of the ROC curve (Figure 7a) is 0.745 ± 0.086 , which was produced by a ROC curve fitting program based on the maximum likelihood estimation method (ROCKIT, <http://metz-roc.uchicago.edu/>, University of Chicago). Figure 7b shows the confusion matrix by choosing 0 as the threshold for the decision scores to generate the corresponding prediction result. As can be seen, out of the 10 cases predicted as "Yes", 7 of them were true responders confirmed through post-therapy CT imaging, yielding a positive predictive value (PPV) of 70% (7/10). On the other hand, among the 32 cases predicted to be "No" by the model, 7 cases were confirmed as responders, corresponding to a negative prediction value (NPV) of 78.1% (25/32). Based on above calculations, the total accuracy (ACC) of the prediction reaches to 76.2% (32/42).

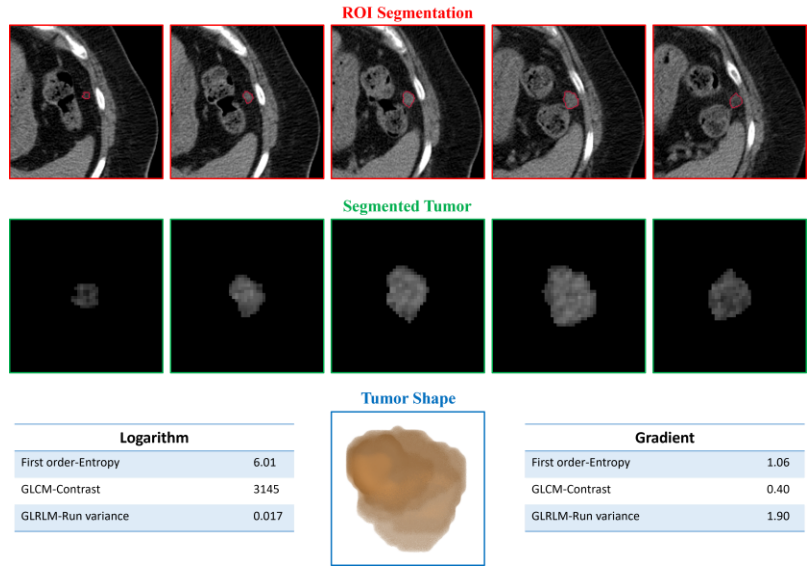


Fig. 2. One example of tumor segmentation and example of extracted features .

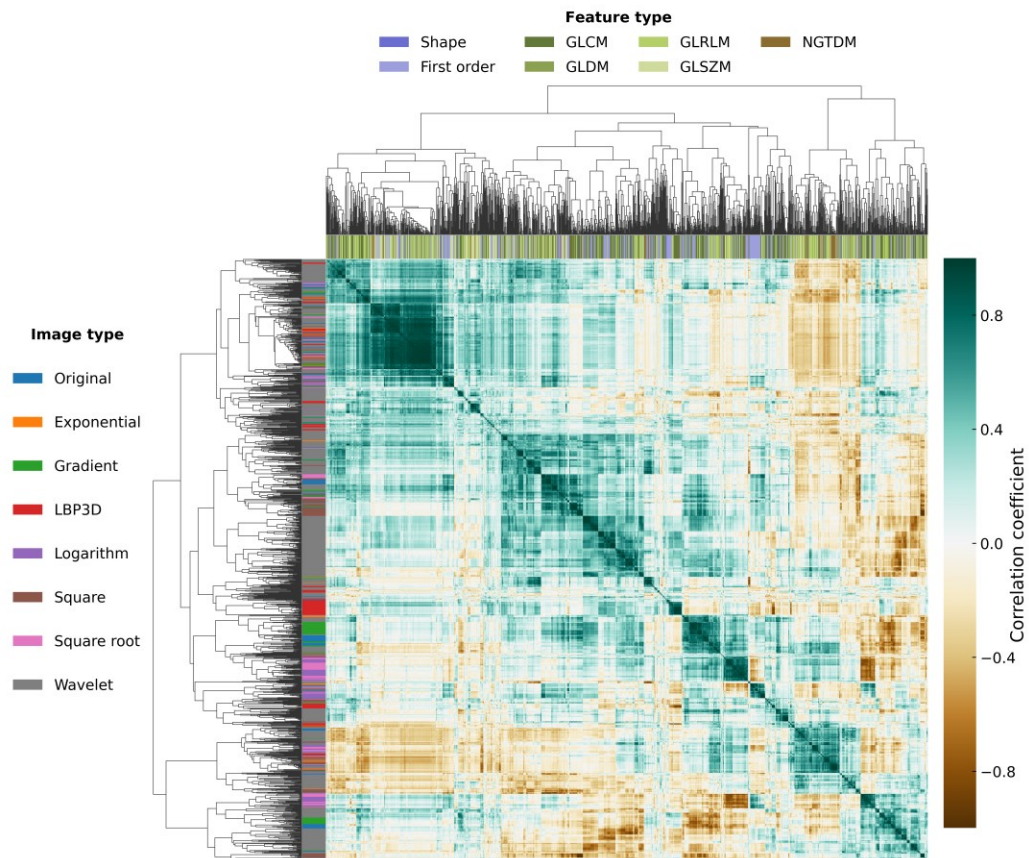


Fig. 3. The hierarchically clustered heatmap of Pearson's correlation coefficients between the extracted 1373 features.

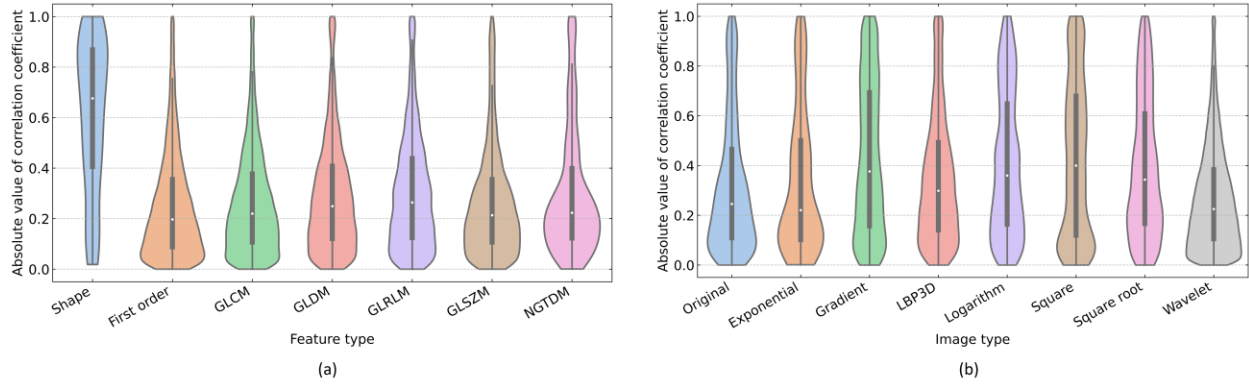


Fig. 4. The distribution of the absolute value of Pearson's correlation coefficients between features of the same feature type or image type.

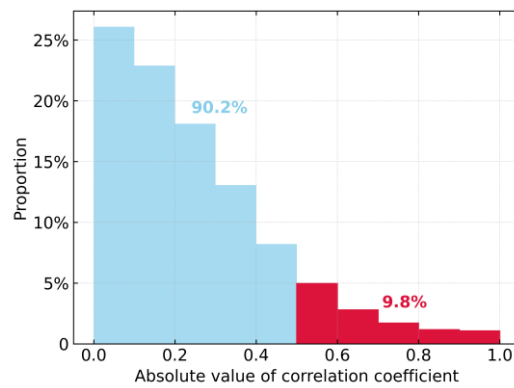


Fig.5. The histogram of the absolute value of correlation coefficients between the extracted 1373 features.

Table 2. The prediction performances of the models trained with different type of features.

	AUC	ACC
Shape	0.617 ± 0.095	64.3 %
First order	0.559 ± 0.096	66.7 %
GLCM	0.633 ± 0.094	64.3 %
GLDM	0.408 ± 0.092	52.4 %
GLRLM	0.454 ± 0.094	59.5 %
GLSZM	0.638 ± 0.094	71.4 %
NGTDM	0.523 ± 0.096	38.1 %

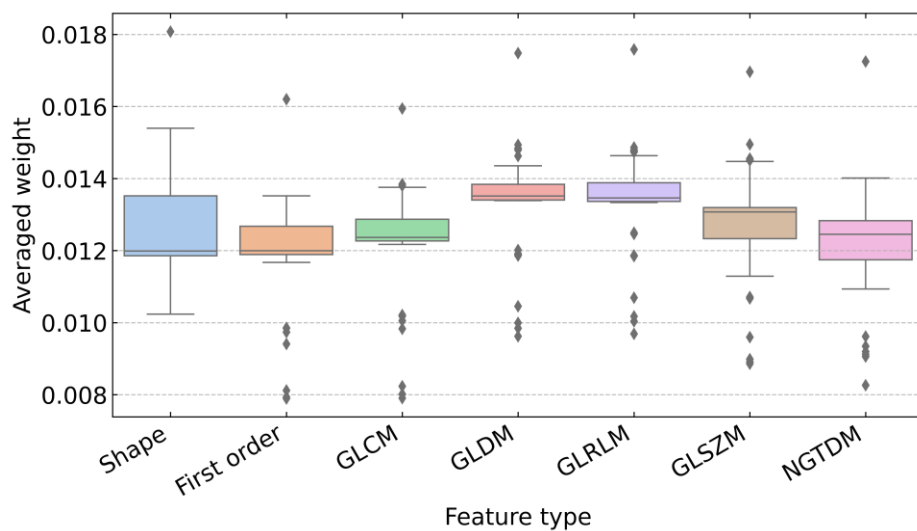


Fig. 6. Averaged weight of each feature type on the PCA-generated new features in the model trained with 1373 features.

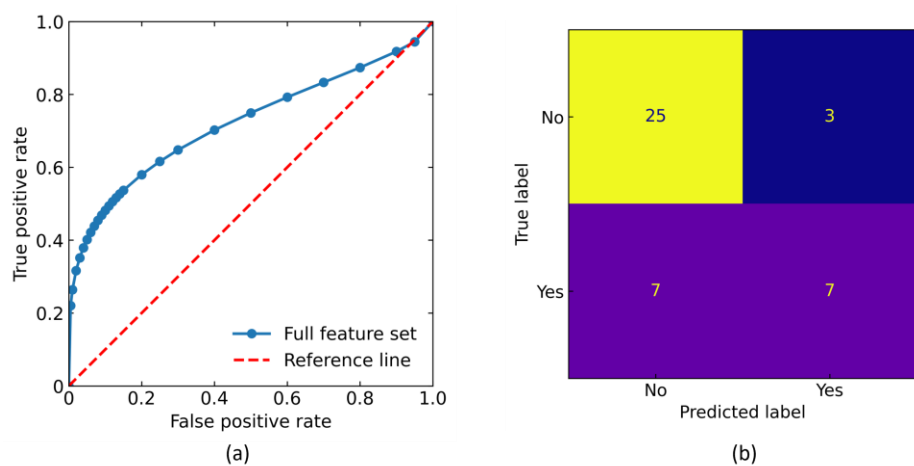


Fig. 7. The ROC curve and confusion matrix for the model trained with 1373 features.

4. DISCUSSION

In this investigation, a novel image marker was developed and initially validated, which aims to predict the tumor responses to neoadjuvant chemotherapy (NACT) in ovarian cancer. This study follows one pioneering research which utilized the radiomics on NACT effectiveness evaluation for advanced stage ovarian cancer patients [51]. Historic CT image based NACT prognostic models are based on the visual findings on the presence of malignancy sites (e.g. pleural effusion or mesentery deposits [19]) and some simple measurement depicted on the acquired images (e.g. tumor diameters [52, 53]). Despite the association between these features and cytoreduction, this method suffers from the inter- and intra- radiologist variability and time-varied diagnostic criteria [20, 54], which causes low robustness and unsatisfactory performance. In our study, a large number of radiomics features were computed on the tumors to quantify the copious prognostic information. Followed by the PCA and SVM, this information was further extracted and identified to generate a single clinical marker for outcome prediction. Using a dataset containing 42 ovarian cancer patients, the marker achieved an overall accuracy of 76.2%. The results indicate that the CT images contain clinically meaningful prognostic information, which can be effectively extracted and integrated by radiomics method. In addition, as compared to the other investigated molecular markers, our proposed method will not create additional financial burdens on the patients, as CT imaging is the routine examination for ovarian cancer patients.

Second, we computed a total of 1373 radiomics features for NACT response prediction. To the best of our knowledge, this is by far the largest feature pool for this specific medical imaging task. All these features can be divided into three different groups (e.g. shape, intensity, and texture). The result shows the five subcategories of texture features has controversial performance on this task: only GLSZM and GLCM indicate significant discriminative power on classifying responders and non-responders (Table 2). Given that these two texture feature subgroups describe the connected or co-occurrence zones with the same grayscale level, it implies the NACT tumor responses or resistance is more sensitive to such an intensity change. However, in the final feature cluster, all these features demonstrate an approximately equal contribution, which may be attributed by the fact that the features from different groups provide complementary information to the final marker. This observation also implies the necessity of radiomics method: each of these computed 1373 features characterizes the tumor heterogeneity uniquely, which is highly desirable in generating the final marker.

Despite the encouraging results, we acknowledge that the study has the following limitations. First, the dataset only contains 42 patients from a single institution. The performance and robustness of our proposed algorithm should be further verified on a comprehensive multiple-institution database with diversified patients. Second, the model is developed based on conventional SVM classifier, and only radiomics features were used. Some emerging technologies such as deep learning [55, 56] were not adopted. One possible improvement of this study would be to combine the radiomics and deep learning features together to further enhance the prediction accuracy. Third, only CT image information was utilized. Other widely available information, such as pathologic image, and clinical factors, were not considered. Fusing all these information together will help us improve the model performance. Despite these limitations, this investigation offers valuable information for precision treatment in future clinical practice.

ACKNOWLEDGEMENTS

We acknowledge the support from the following funding agencies: National Institute of General Medical Sciences (NIGMS, Sub-project 8620, P20GM135009-02), Oklahoma Center for Advancement of Science and Technology (OCAST HR23-122).

REFERENCES

- [1] R.L. Siegel, K.D. Miller, N.S. Wagle, A. Jemal, Cancer statistics, 2023, CA: A Cancer Journal for Clinicians, 73 (2023) 17-48.
- [2] C.L.P. Slatnik, E. Duff, Ovarian cancer: Ensuring early diagnosis, The Nurse Practitioner, 40 (2015) 47-54.
- [3] B.T. Hennessy, R.L. Coleman, M. Markman, Ovarian cancer, The Lancet, 374 (2009) 1371-1382.
- [4] S.B. Dewdney, B.J. Rimel, A.J. Reinhart, N.T. Kizer, R.A. Brooks, L.S. Massad, I. Zigelboim, The role of neoadjuvant chemotherapy in the management of patients with advanced stage ovarian cancer: Survey results from members of the Society of Gynecologic Oncologists, Gynecol. Oncol., 119 (2010) 18-21.
- [5] Y. Ansquer, E. Leblanc, K. Clough, P. Morice, J. Dauplat, P. Mathevet, C. Lhommé, C. Scherer, J.-D. Tigaud, M. Benchaib, E. Fourme, D. Castaigne, D. Querleu, D. Dargent, Neoadjuvant chemotherapy for unresectable ovarian carcinoma, Cancer, 91 (2001) 2329-2334.
- [6] J.A. Rauh-Hain, N. Rodriguez, W.B. Growdon, A.K. Goodman, D.M. Boruta, N.S. Horowitz, M.G. del Carmen, J.O. Schorge, Primary Debulking Surgery Versus Neoadjuvant Chemotherapy in Stage IV Ovarian Cancer, Annals of Surgical Oncology, 19 (2012) 959-965.
- [7] C.L. Fagö-Olsen, B. Ottesen, H. Kehlet, S.L. Antonsen, I.J. Christensen, A. Markauskas, B.J. Mosgaard, C. Ottosen, C.H. Soegaard, E. Soegaard-Andersen, C. Hoegdall, Does neoadjuvant chemotherapy impair long-term survival for ovarian cancer patients? A nationwide Danish study, Gynecol. Oncol., 132 (2014) 292-298.
- [8] J.J. Mueller, Q.C. Zhou, A. Iasonos, R.E. O'Cearbhaill, F.A. Alvi, A. El Haraki, A.G.Z. Eriksson, G.J. Gardner, Y. Sonoda, D.A. Levine, C. Aghajanian, D.S. Chi, N.R. Abu-Rustum, O. Zivanovic, Neoadjuvant chemotherapy and primary debulking surgery utilization for advanced-stage ovarian cancer at a comprehensive cancer center, Gynecol. Oncol., 140 (2016) 436-442.
- [9] M.A. Glasgow, H. Yu, T.J. Rutherford, M. Azodi, D.-A. Silasi, A.D. Santin, P.E. Schwartz, Neoadjuvant chemotherapy (NACT) is an effective way of managing elderly women with advanced stage ovarian cancer (FIGO Stage IIIC and IV), Journal of Surgical Oncology, 107 (2013) 195-200.
- [10] P.E. Schwartz, T.J. Rutherford, J.T. Chambers, E.I. Kohorn, R.P. Thiel, Neoadjuvant Chemotherapy for Advanced Ovarian Cancer: Long-Term Survival, Gynecol. Oncol., 72 (1999) 93-99.
- [11] M.J. Worley, S.H. Guseh, J.A. Rauh-Hain, K.A. Williams, M.G. Muto, C.M. Feltmate, R.S. Berkowitz, N.S. Horowitz, Does neoadjuvant chemotherapy decrease the risk of hospital readmission following debulking surgery?, Gynecol. Oncol., 129 (2013) 69-73.
- [12] J.Y. Hou, M.G. Kelly, H. Yu, J.N. McAlpine, M. Azodi, T.J. Rutherford, P.E. Schwartz, Neoadjuvant chemotherapy lessens surgical morbidity in advanced ovarian cancer and leads to improved survival in stage IV disease, Gynecol. Oncol., 105 (2007) 211-217.
- [13] M. Moschetta, S. Boussios, E. Rassy, E.P. Samartzis, G. Funingana, M. Uccello, Neoadjuvant treatment for newly diagnosed advanced ovarian cancer: where do we stand and where are we going?, Ann Transl Med, 8 (2020) 1710.
- [14] R. Cowan, D. Chi, S. Kehoe, M. Nankivell, A. Leary, Primary Surgery or Neoadjuvant Chemotherapy in Advanced Ovarian Cancer: The Debate Continues..., American Society of Clinical Oncology Educational Book, (2016) 153-162.

- [15] S. Sato, H. Itamochi, Neoadjuvant chemotherapy in advanced ovarian cancer: latest results and place in therapy, *Ther Adv Med Oncol*, 6 (2014) 293-304.
- [16] J. Liu, X. Jiao, Q. Gao, Neoadjuvant chemotherapy-related platinum resistance in ovarian cancer, *Drug Discov. Today*, 25 (2020) 1232-1238.
- [17] P. Tajik, R.v.d. Vrie, M.H. Zafarmand, C. Coens, M.R. Buist, I. Vergote, P.M.M. Bossuyt, G.G. Kenter, The FIGO Stage IVA Versus IVB of Ovarian Cancer: Prognostic Value and Predictive Value for Neoadjuvant Chemotherapy, *International Journal of Gynecologic Cancer*, 28 (2018) 453-458.
- [18] R. Cioffi, A. Bergamini, E. Rabaiotti, M. Petrone, F. Pella, D. Ferrari, G. Mangili, M. Candiani, Neoadjuvant chemotherapy in high-risk ovarian cancer patients: Role of age, *Tumori Journal*, 105 (2019) 168-173.
- [19] A. Patel, P. Iyer, S. Matsuzaki, K. Matsuo, A.K. Sood, N.D. Fleming, Emerging Trends in Neoadjuvant Chemotherapy for Ovarian Cancer, *Cancers*, 13 (2021) 626.
- [20] R.S. Suidan, P.T. Ramirez, D.M. Sarasohn, J.B. Teitcher, S. Mironov, R.B. Iyer, Q. Zhou, A. Iasonos, H. Paul, M. Hosaka, C.A. Aghajanian, M.M. Leitao, G.J. Gardner, N.R. Abu-Rustum, Y. Sonoda, D.A. Levine, H. Hricak, D.S. Chi, A multicenter prospective trial evaluating the ability of preoperative computed tomography scan and serum CA-125 to predict suboptimal cytoreduction at primary debulking surgery for advanced ovarian, fallopian tube, and peritoneal cancer, *Gynecol. Oncol.*, 134 (2014) 455-461.
- [21] D. Zhang, Y.-x. Jiang, S.-j. Luo, R. Zhou, Q.-x. Jiang, H. Linghu, Serum CA125 levels predict outcome of interval debulking surgery after neoadjuvant chemotherapy in patients with advanced ovarian cancer, *Clinica Chimica Acta*, 484 (2018) 32-35.
- [22] K. Oikonomopoulou, L. Li, Y. Zheng, I. Simon, R.L. Wolfert, D. Valik, M. Nekulova, M. Simickova, T. Frgala, E.P. Diamandis, Prediction of ovarian cancer prognosis and response to chemotherapy by a serum-based multiparametric biomarker panel, *British Journal of Cancer*, 99 (2008) 1103-1113.
- [23] Y. Shen, L. Li, Serum HE4 superior to CA125 in predicting poorer surgical outcome of epithelial ovarian cancer, *Tumor Biology*, 37 (2016) 14765-14772.
- [24] Y.-W. Huang, Association of BRCA1/2 mutations with ovarian cancer prognosis: An updated meta-analysis, *Medicine*, 97 (2018) e9380.
- [25] Y.L. Liu, O.T. Filippova, Q. Zhou, A. Iasonos, D.S. Chi, O. Zivanovic, Y. Sonoda, G.J. Gardner, V.A. Broach, R.E. O'Cearbhaill, J.A. Konner, C. Aghajanian, K. Long Roche, W.P. Tew, Characteristics and survival of ovarian cancer patients treated with neoadjuvant chemotherapy but not undergoing interval debulking surgery, *JGO*, 31 (2019) 0-0.
- [26] L. Fass, Imaging and cancer: A review, *Molecular Oncology*, 2 (2008) 115-152.
- [27] S. Kyriazi, S.B. Kaye, N.M. deSouza, Imaging ovarian cancer and peritoneal metastases—current and emerging techniques, *Nat. Rev. Clin. Oncol.*, 7 (2010) 381-393.
- [28] Y. Qiu, M. Tan, S. McMeekin, T. Thai, K. Ding, K. Moore, H. Liu, B. Zheng, Early prediction of clinical benefit of treating ovarian cancer using quantitative CT image feature analysis, *Acta Radiol.*, 57 (2016) 1149-1155.
- [29] M.E. Mayerhoefer, A. Materka, G. Langs, I. Häggström, P. Szczypiński, P. Gibbs, G. Cook, Introduction to Radiomics, *J. Nucl. Med.*, 61 (2020) 488-495.
- [30] P. Lambin, R.T.H. Leijenaar, T.M. Deist, J. Peerlings, E.E.C. de Jong, J. van Timmeren, S. Sanduleanu, R.T.H.M. Larue, A.J.G. Even, A. Jochems, Y. van Wijk, H. Woodruff, J. van Soest, T. Lustberg, E. Roelofs, W. van Elmpt, A. Dekker, F.M. Mottaghy, J.E. Wildberger, S. Walsh, Radiomics: the bridge between medical imaging and personalized medicine, *Nat. Rev. Clin. Oncol.*, 14 (2017) 749-762.
- [31] J.E. van Timmeren, D. Cester, S. Tanadini-Lang, H. Alkadhi, B. Baessler, Radiomics in medical imaging—“how-to” guide and critical reflection, *Insights Imaging*, 11 (2020) 91.
- [32] G. Danala, Y. Wang, T. Thai, C. Gunderson, K. Moxley, K. Moore, R. Mannel, S. Cheng, H. Liu, B. Zheng, Y. Qiu, Improving efficacy of metastatic tumor segmentation to facilitate early prediction of ovarian cancer patients' response to chemotherapy, *SPiE2017*.

- [33] J.J.M. van Griethuysen, A. Fedorov, C. Parmar, A. Hosny, N. Aucoin, V. Narayan, R.G.H. Beets-Tan, J.C. Fillion-Robin, S. Pieper, H. Aerts, Computational Radiomics System to Decode the Radiographic Phenotype, *Cancer Res*, 77 (2017) e104-e107.
- [34] R.M. Haralick, Statistical and structural approaches to texture, *Proceedings of the IEEE*, 67 (1979) 786-804.
- [35] C. Sun, W.G. Wee, Neighboring gray level dependence matrix for texture classification, *Computer Vision, Graphics, and Image Processing*, 23 (1983) 341-352.
- [36] M.M. Galloway, Texture analysis using gray level run lengths, *Computer Graphics and Image Processing*, 4 (1975) 172-179.
- [37] G. Thibault, B. Fertil, C. Navarro, L., S. Pereira, P. Cau, N. Lévy, J. Sequeira, J.-L. Mari, Texture indexes and gray level size zone matrix. Application to cell nuclei classification, 10th International Conference on Pattern Recognition and Information Processing, PRIP 2009Minsk, Belarus, 2009, pp. 140--145.
- [38] M. Amadasun, R. King, Textural features corresponding to textural properties, *IEEE Transactions on Systems, Man, and Cybernetics*, 19 (1989) 1264-1274.
- [39] F. Pedregosa, G. Varoquaux, A. Gramfort, V. Michel, B. Thirion, O. Grisel, M. Blondel, P. Prettenhofer, R. Weiss, V. Dubourg, J. Vanderplas, A. Passos, D. Cournapeau, M. Brucher, M. Perrot, É. Duchesnay, Scikit-learn: Machine Learning in Python, *J. Mach. Learn. Res.*, 12 (2011) 2825–2830.
- [40] A. Fernandez, S. Garcia, F. Herrera, N.V. Chawla, SMOTE for Learning from Imbalanced Data: Progress and Challenges, Marking the 15-year Anniversary, *J. Artif. Intell. Res.*, 61 (2018) 863-905.
- [41] H. Abdi, L.J. Williams, Principal component analysis, *WIREs Computational Statistics*, 2 (2010) 433-459.
- [42] C. Olivier, S. Bernhard, Z. Alexander, Spectral Methods for Dimensionality Reduction, *Semi-Supervised Learning*, MIT Press 2006, pp. 293-308.
- [43] M. Awad, R. Khanna, Support Vector Machines for Classification, in: M. Awad, R. Khanna (Eds.) *Efficient Learning Machines: Theories, Concepts, and Applications for Engineers and System Designers*, Apress, Berkeley, CA, 2015, pp. 39-66.
- [44] J. Cervantes, F. Garcia-Lamont, L. Rodríguez-Mazahua, A. Lopez, A comprehensive survey on support vector machine classification: Applications, challenges and trends, *Neurocomputing*, 408 (2020) 189-215.
- [45] S. Varma, R. Simon, Bias in error estimation when using cross-validation for model selection, *BMC Bioinformatics*, 7 (2006) 91.
- [46] R.B. Rao, G. Fung, R. Rosales, On the Dangers of Cross-Validation. An Experimental Evaluation, *Proceedings of the 2008 SIAM International Conference on Data Mining (SDM)*, pp. 588-596.
- [47] A.M. Molinaro, R. Simon, R.M. Pfeiffer, Prediction error estimation: a comparison of resampling methods, *Bioinformatics*, 21 (2005) 3301-3307.
- [48] S.H. Park, J.M. Goo, C.-H. Jo, Receiver Operating Characteristic (ROC) Curve: Practical Review for Radiologists, *Korean J Radiol*, 5 (2004) 11-18.
- [49] A.P. Bradley, The use of the area under the ROC curve in the evaluation of machine learning algorithms, *Pattern Recognit.*, 30 (1997) 1145-1159.
- [50] L. Wilkinson, M. Friendly, The History of the Cluster Heat Map, *The American Statistician*, 63 (2009) 179-184.
- [51] L. Rundo, L. Beer, L. Escudero Sanchez, M. Crispin-Ortuzar, M. Reinius, C. McCague, H. Sahin, V. Bura, R. Pintican, M. Zerunian, S. Ursprung, I. Allajbeu, H. Addley, P. Martin-Gonzalez, T. Buddenkotte, N. Singh, A. Sahdev, I.-G. Funingana, M. Jimenez-Linan, F. Markowetz, J.D. Brenton, E. Sala, R. Woitek, Clinically Interpretable Radiomics-Based Prediction of Histopathologic Response to Neoadjuvant Chemotherapy in High-Grade Serous Ovarian Carcinoma, *Frontiers in Oncology*, 12 (2022).
- [52] T. Vallius, J. Hynninen, J. Kemppainen, V. Alves, K. Auranen, J. Matomäki, S. Oksa, J. Virtanen, S. Grénman, A. Auranen, M. Seppänen, 18F-FDG-PET/CT based total metabolic tumor volume change

during neoadjuvant chemotherapy predicts outcome in advanced epithelial ovarian cancer, *Eur. J. Nucl. Med. Mol. Imaging*, 45 (2018) 1224-1232.

[53] E.A. Eisenhauer, P. Therasse, J. Bogaerts, L.H. Schwartz, D. Sargent, R. Ford, J. Dancey, S. Arbuck, S. Gwyther, M. Mooney, L. Rubinstein, L. Shankar, L. Dodd, R. Kaplan, D. Lacombe, J. Verweij, New response evaluation criteria in solid tumours: Revised RECIST guideline (version 1.1), *Eur. J. Cancer*, 45 (2009) 228-247.

[54] M. Krasovitsky, Y.C. Lee, H.-W. Sim, T. Chawla, H. Moore, D. Moses, L. Baker, C. Mandel, A. Kielar, A. Hartery, M. O'Malley, M. Friedlander, A.M. Oza, L. Wang, S. Lheureux, M. Wilson, Interobserver and intraobserver variability of RECIST assessment in ovarian cancer, *International Journal of Gynecologic Cancer*, 32 (2022) 656-661.

[55] X. Chen, X. Wang, K. Zhang, K.-M. Fung, T.C. Thai, K. Moore, R.S. Mannel, H. Liu, B. Zheng, Y. Qiu, Recent advances and clinical applications of deep learning in medical image analysis, *Med. Image Anal.*, 79 (2022) 102444.

[56] J. Li, J. Chen, Y. Tang, C. Wang, B.A. Landman, S.K. Zhou, Transforming medical imaging with Transformers? A comparative review of key properties, current progresses, and future perspectives, *Med. Image Anal.*, 85 (2023) 102762.